J Solid State Electrochem (2012) 16:1999–2004
DOI 10.1007/s10008-011-1602-6

ORIGINAL PAPER

Synthesis and electrochemical properties of graphene-SnS_2 nanocomposites for lithium-ion batteries

Chenfei Shen · Luyao Ma · Mingbo Zheng · Bin Zhao · Danfeng Qiu · Lijia Pan · Jieming Cao · Yi Shi

Received: 8 August 2011 / Revised: 12 November 2011 / Accepted: 18 November 2011 / Published online: 8 December 2011

Abstract Graphene-SnS_2 nanocomposites were prepared via a solvothermal method with different loading of SnS_2. The nanostructure and morphology of the samples were characterized by X-ray diffraction (XRD), scanning electron microscopy (SEM), and transmission electron microscopy (TEM). The XRD patterns revealed that hexagonal SnS_2 was obtained. SEM and TEM results indicated that SnS_2 particles distributed homogeneously on graphene sheets. The electrochemical properties of the samples as active anode materials for lithium-ion batteries were examined by constant current charge–discharge cycling. The composite with weight ratio between graphene and SnS_2 of 1:4 had the highest rate capability among all the samples and its reversible capacity after 50 cycles was 351 mAh/g, which was much higher than that of the pure SnS_2 (23 mAh/g). With graphene as conductive matrix, homogeneous distribution of SnS_2 nanoparticles can be ensured and volume changes of the nanoparticles during the charge and discharge processes can be accomodated effectively, which results in good electrochemical performance of the composites.

Keywords SnS_2 · Graphene · Solvothermal synthesis · Lithium-ion battery

C. Shen · L. Ma · M. Zheng (✉) · B. Zhao · D. Qiu · L. Pan · Y. Shi (✉)
National Laboratory of Microstructures,
School of Electronic Science and Engineering, Nanjing University,
Nanjing 210093, China
e-mail: zhengmingbo@nju.edu.cn
e-mail: yshi@nju.edu.cn

C. Shen · J. Cao
Nanomaterials Research Institute,
College of Materials Science and Technology,
Nanjing University of Aeronautics and Astronautics,
Nanjing 210016, China

Introduction

Rechargeable lithium-ion batteries are currently the predominant power sources for portable electronic devices. To achieve improved electrochemical performance, new anode materials have been studied extensively. Among them, Li–Sn alloy compounds have attracted great interest due to their theoretical specific capacity up to 992 mAh/g [1]. SnS_2 was reported to be used as a novel anode material for lithium-ion batteries as it transforms to Li–Sn alloys during charge–discharge process [2, 3]. However, even though SnS_2 exhibits high initial discharge capacity, the large volume changes and loss of electrical contact during lithium intercalation and deintercalation result in capacity fading of the compound. Several approaches can be considered to enhance the capacity retention, such as reducing the particle size to nanoscale or dispersing the electroactive particles in a carbon matrix. It is believed that carbon matrix can buffer the volume changes and improve the electronic and ionic conductivities [4].

Graphene, which consists of two-dimensional sheets of covalently bonded carbon atoms, offers great advantages owing to its high surface area, good conductivity, and good mechanical properties [5, 6]. It is believed that the restacking of graphene nanosheets will be effectively prevented with nanosize particles deposited between them. Besides, the aggregation and pulverization of the active particle on cycling will be suppressed [7]. For these reasons, graphene has been studied as conductive matrix of lithium-ion battery electrode materials [8–10]. In this paper, we utilized functionalized graphene sheets (FGS) [11] as matrix to synthesize graphene-SnS_2 nanocomposites as lithium-ion battery anode materials via a solvothermal method. On this basis, we synthesized the nanocomposites with different loading of SnS_2. The obtained products exhibited enhanced cycle performance and lithium storage capacity compared with pure SnS_2 and FGS.

Experimental

Preparation of FGS

Graphite oxide (GO) was prepared by Hummers method [12]. To obtain FGS, certain amount of GO was thermally exfoliated at 300 °C for 5 min under air atmosphere and subsequently treated at 900 °C in N_2 for 3 h with a heating rate of 2 °C/min. The obtained sample was denoted as FGS.

Preparation of graphene-SnS_2 nanocomposites

All of the reactants and solvents were of analytical grade and were used without any further purification. To synthesize graphene-SnS_2 nanocomposite with theoretical weight ratio between FGS and SnS_2 of 1:1, FGS (100 mg) and $SnCl_4{\cdot}5H_2O$ (192 mg) were added in 100 mL of ethylene glycol. After stirring for 15 min, 164 mg of thioacetamide was dissolved in 10 mL of ethylene glycol and dropped into the mixture. After ultrasonication for 30 min, the mixture was transferred into a 150-mL Teflon-lined stainless steel autoclave. The autoclave was sealed and maintained at 190 °C for 12 h, and then allowed to cool to room temperature. The obtained black product was collected, washed with ethanol and distilled water several times, and dried under vacuum at 50 °C for 12 h. The obtained sample was denoted as GS1.

Parallel experiments were carried out to synthesize graphene-SnS_2 nanocomposites with theoretical weight ratio between FGS and SnS_2 of 1:2 and 1:4. The obtained samples were denoted as GS2 and GS3, respectively. For comparison, pure SnS_2 nanoparticles were also prepared according to the process described above with the exception of FGS as support.

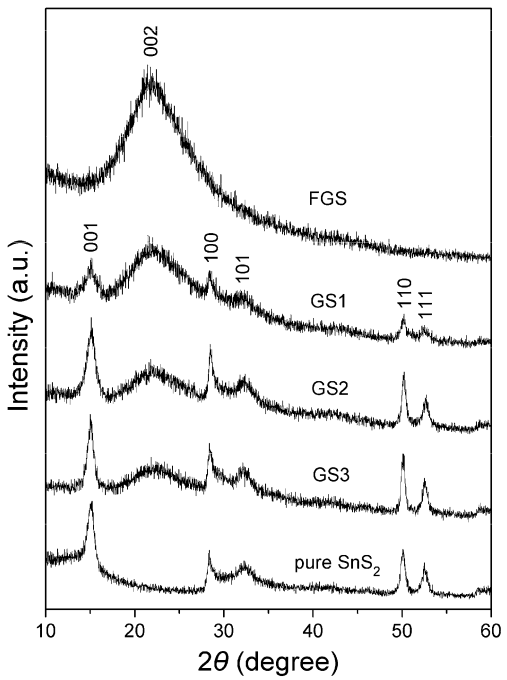

Fig. 1 XRD patterns of FGS, GS1 (FGS to SnS_2=1:1), GS2 (FGS to SnS_2=1:2), GS3 (FGS to SnS_2=1:4), and pure SnS_2 nanoparticles

Characterization

The dimension and morphology of the samples were observed by scanning electron microscopy (SEM) (Gemini LEO1530) and transmission electron microscopy (TEM) (JEOL JEM-2100). X-ray diffraction patterns were performed by a Bruker D8-Advance diffractometer equipped with graphite-monochromatized Cu Kα, radiation (λ=0.15418 nm).

A two-electrode potentiostatic system with graphene-SnS_2 nanocomposites as the working electrode was used to carry out the electrochemical studies using lithium foil as the reference and counter electrodes. The working electrodes were prepared with graphene-SnS_2 nanocomposites as the active material and poly (vinylidene fluoride) as the binder, mixed by the weight ratio of 9:1, and dissolved in 1-methyl-2-pyrrolidinone to form a slurry. The mixture slurry was spread onto copper foil, dried in vacuum, and then pressed for use as the working electrode (the loading of pure active material was 2 mg/cm^2). The coin cells were fabricated under an Ar-filled glove box, consisted of Li foil as the reference and counter electrodes and polyethylene film (Celgard 2300) as the separator. The electrolyte was 1 M $LiPF_6$ dissolved in an ethylene carbonate and diethyl carbonate (1:1 vol) mixture. The cells were charged and discharged at a constant current density of 200 mA/g between 0.01 and 1.2 V (vs. Li^+/Li).

Results and discussion

Figure 1 shows the X-ray diffraction (XRD) patterns of FGS, GS1, GS2, GS3, and pure SnS_2 nanoparticles. The feature diffraction peak of FGS appears at 23° and the peak could also be observed in the figures of GS1, GS2, and GS3. The XRD pattern of pure SnS_2 matches well that of hexagonal SnS_2 (JCPDS card, no. 23-0677) and the diffraction peaks corresponding to (001), (100), (101), (110), and (111) planes of hexagonal SnS_2 could also be observed in GS1, GS2, and GS3.

Figure 2a, e shows the morphology characterization of FGS. Both images indicate that the sample has wrinkled paper-like structure and the nanopores of FGS could be observed in Fig. 2a. In the SEM images of GS1 (Fig. 2b), GS2 (Fig. 2c), and GS3 (Fig. 2d), the wrinkles of FGS could also be observed. Besides, SnS_2 particles were observed to be intercalated into the nanopores of FGS. SnS_2 nanoparticles were well spread out on graphene sheets in all the three

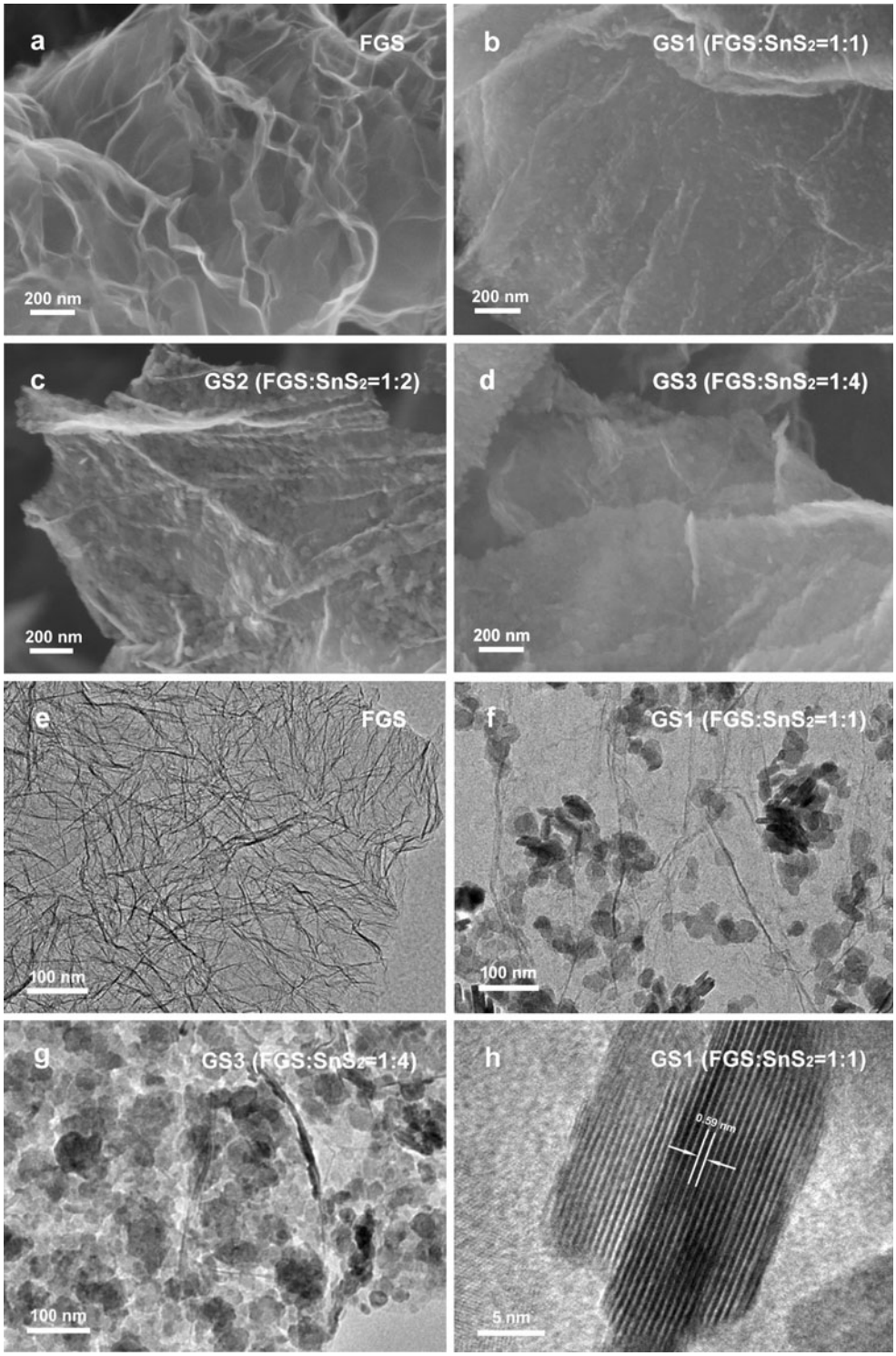

Fig. 2 SEM images of **a** FGS, **b** GS1, **c** GS2, and **d** GS3; TEM images of **e** FGS, **f** GS1, and **g** GS3; **h** HRTEM image of GS1

samples. The homogeneous distribution of SnS_2 particles on graphene sheets could contribute to buffering the volume expansion of SnS_2 particles during the charge and discharge processes. Subpanels f and g in Fig. 2 are TEM images of GS1 and GS3, respectively. In Fig. 2f, round and plate-shaped SnS_2 nanoparticles with an average size of about 30 nm were observed to be decorated on graphene. Besides, the figure demonstrates relatively low loading of SnS_2 in GS1. On the contrary, the TEM image of GS3 (Fig. 2g) shows that the composite consisted of graphene sheets heavily decorated with SnS_2 nanoparticles. Due to high loading of SnS_2 in GS3, there were hardly large areas of graphene

sheets without SnS_2 decoration. By comparing Fig. 2e with Fig. 2g, it is obvious that the restacking of graphene sheets was effectively prevented with SnS_2 nanoparticles intercalated between graphene sheets. The high active surface area of graphene was therefore kept, which is favorable for increasing the lithium storage capacity of graphene in the composites [13]. The HRTEM image of GS1 (Fig. 2h) shows the lattice spacing of about 0.59 nm, which corresponds to (001) plane of hexagonal SnS_2.

Figure 3 shows the first 2 cycle's charge–discharge curves of FGS, GS1, GS2, GS3, and pure SnS_2, which were measured between 0.01 and 1.2 V vs. Li^+/Li at a current density of 200 mA/g. The red and green curves represent first and second charge–discharge process, respectively. A two-step electrochemical reaction mechanism of SnS_2 with lithium has been proposed as reported [14, 15]:

$$SnS_2 + 4Li^+ + 4e^- \rightarrow Sn + 2Li_2S \quad (1)$$

$$Sn + xLi^+ + xe^- \leftrightarrow Li_xSn(0 \le x \le 4.4). \quad (2)$$

In the first discharge process of GS1, GS2, GS3, and pure SnS_2, the irreversible plateau emerged at about 1.2 V. It was

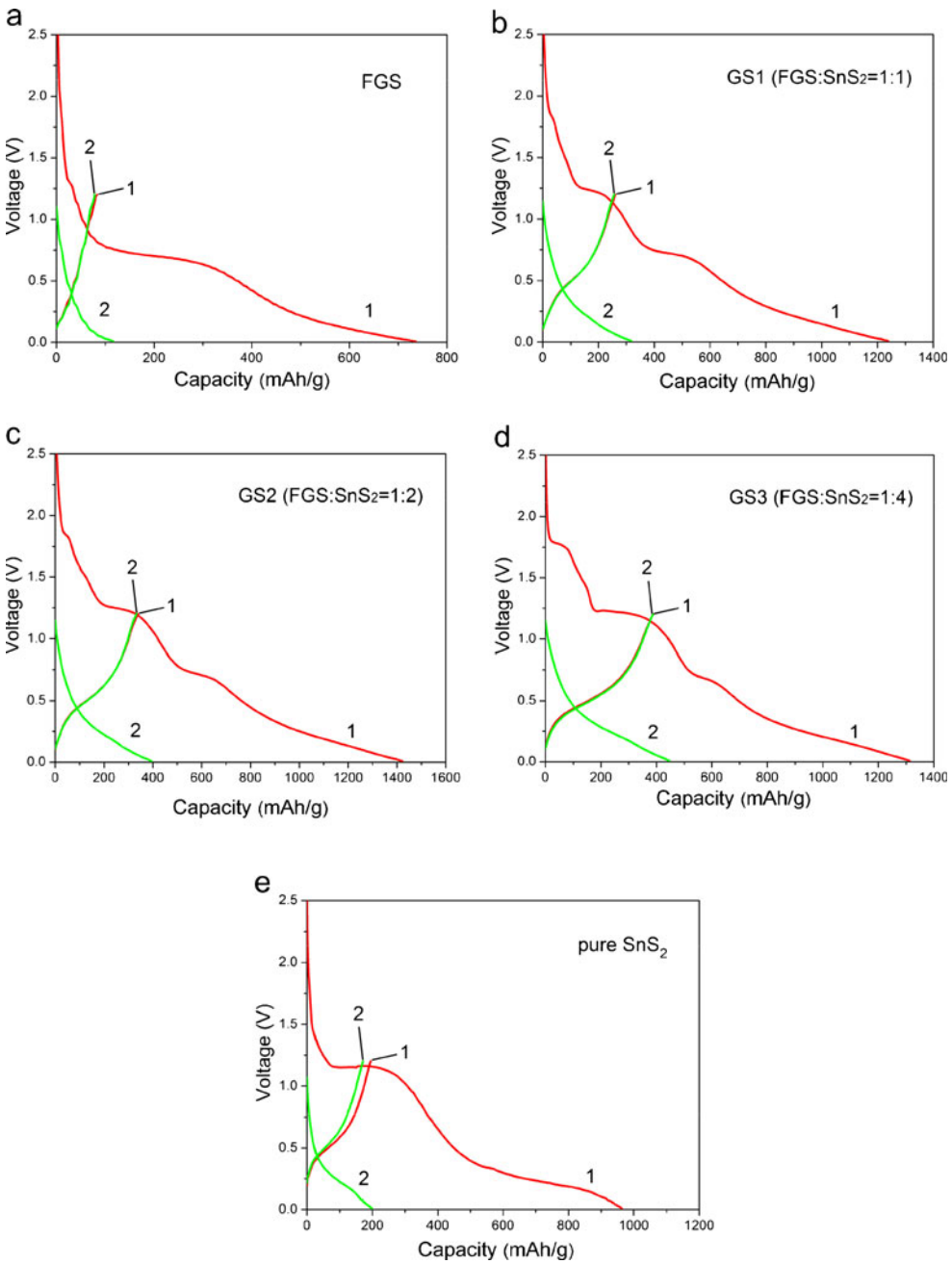

Fig. 3 Charge–discharge curves of **a** FGS, **b** GS1, **c** GS2, **d** GS3, and **e** pure SnS_2 at a current density of 200 mA/g

assigned to the decomposition of the SnS_2 nanoparticles into Sn and Li_2S as shown by reaction 1. The discharge plateaus in the potential ranges of 0.0–0.5 V represent the formation of Li/Sn alloys and charge plateaus in the potential ranges of 0.5–0.7 V represent the dealloy process, which corresponds to reaction 2. The additional peak at 1.8 V in the first discharge process of samples GS1, GS2, and GS3 is attributed to the lithium intercalation into the SnS_2 layers without phase decomposition. It is possible that the homogeneous distribution of SnS_2 nanoparticles on graphene layers gives rise to high surface area of the particles, which promotes side reactions with the electrolytes and thus leads to lithium intercalation into the SnS_2 layers without phase decomposition. However, the peak was not obvious in the curve of pure SnS_2. It is supposed to be due to the aggregation of pure SnS_2 particles, which reduces their surface areas. In terms of the first discharge curve for FGS, an irreversible plateau was observed at about 0.7 V and it was also observed in the first discharge curves of GS1, GS2, and GS3. It may be related to the formation of a passivation film or solid electrolyte interphase [7, 9].

The initial discharge capacities for GS1, GS2, GS3, and pure SnS_2 were as high as 1,240, 1,420, 1,310, and 963 mAh/g, respectively. It may be due to the high surface-to-volume ratio of the nanostructure and the abundant surface defects, which may accelerate lithium intercalation and side reactions with the electrolytes. The initial efficiencies of these electrodes were calculated to be 21.1%, 23.8%, 29.6%, and 20.1%, respectively. It can be seen that the initial efficiencies increase with the increasing of SnS_2 amount in the composites and the initial efficiency of pure SnS_2 was the minimum among the four samples.

Figure 4 shows the electrochemical cycle properties of FGS, GS1, GS2, GS3, and pure SnS_2 over 50 cycles at a current density of 200 mA/g. It demonstrates that FGS had a good reversible capacity retention (83.1% after 50 cycles); however, the reversible capacity was only about 70 mAh/g. After 50 cycles, the reversible capacity of pure SnS_2 decreased to 23 mAh/g from the initial reversible capacity of 194 mAh/g with the retention of only 11.9%. This could be explained by its large volume changes in the processes of intercalation and deintercalation of lithium ion, which resulted in the pulverization and capacity fading. In contrast to the poor cycle performance of pure SnS_2, the reversible capacities of the graphene-SnS_2 nanocomposites were stable over 50 cycles. The initial reversible capacities for GS1, GS2, and GS3 were 261, 338, and 388 mAh/g, respectively. After 50 cycles, the reversible capacities decreased to 205, 286, and 351 mAh/g, corresponding to 78.5%, 84.6%, and 90.5% retention of the initial reversible capacities for samples GS1, GS2, and GS3, respectively. It can be seen that with FGS as a conductive matrix, the capacities of the samples increase with the increasing of SnS_2 amount in the composites. The improvement in the cycle performance of graphene-SnS_2 nanocomposites compared with pure SnS_2 could be attributed to the buffering and binding effect of FGS on the volume changes of SnS_2 in the charge and discharge processes.

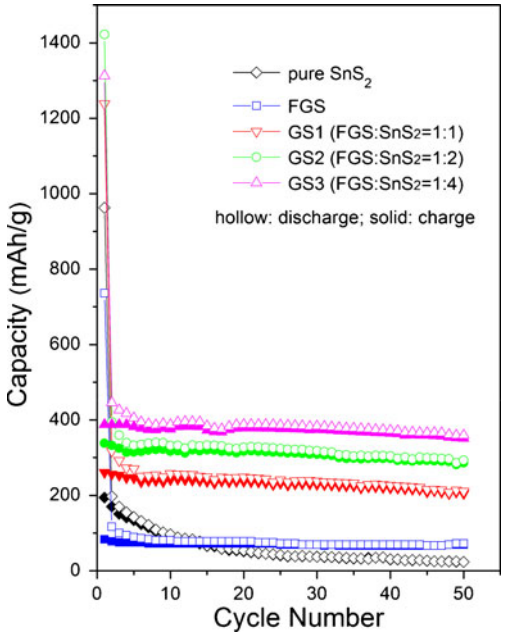

Fig. 4 Variation of specific capacity with cycle number at a current density of 200 mA/g

To further study the rate capability of the samples, GS1, GS2, GS3, and FGS were tested with variable rates (from 100 to 1,000 mA/g) as shown in Fig. 5. At 1,000 mA/g, GS1, GS2, GS3, and FGS retained about 55%, 65%, 75%, and 60% of the initial capacity at 100 mA/g, respectively. It demonstrates that GS3 had the highest charge capacity among the four samples at variable rates and the loss of charge capacity of GS3 was the slowest. It is interesting to note that the rate capability of GS2 and GS3 was higher than that of FGS, besides, the capacity retention of GS2 and GS3 was also higher than that of FGS (Fig. 4). It could be attributed to the synergetic effects between graphene sheets

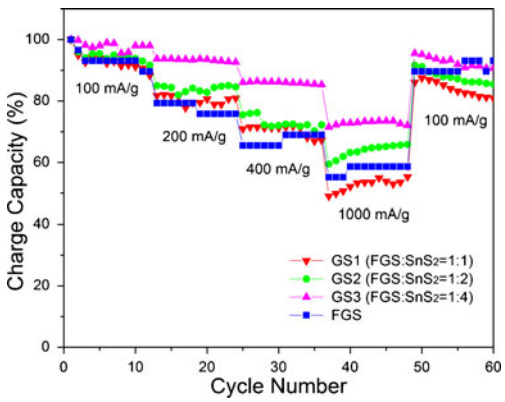

Fig. 5 Rate capability of GS1, GS2, GS3, and FGS

and SnS_2 [13], which can be explained as follows: as two-dimensional matrix, graphene sheets guarantee the homogeneous distribution of SnS_2 nanoparticles and buffer the volume changes of SnS_2. Besides, the good conductivity of graphene sheets makes them good conductive channels. Meanwhile, the SnS_2 nanoparticles between graphene sheets prevent the restacking of graphene sheets effectively, which guarantees the efficient utilization of the good properties of graphene sheets. Graphene sheets and SnS_2 nanoparticles act upon each other and thus results in the enhanced elecrochemical properties of the composites.

Conclusion

In summary, graphene-SnS_2 nanocomposites with different weight ratios between graphene and SnS_2 were synthesized via a solvothermal method. The SEM and TEM characterizations revealed homogeneous distribution of SnS_2 particles on graphene sheets. Electrochemical tests of the composites as lithium-ion battery anode materials demonstrated that the capacity and cycle performance of the samples increased with the increasing of SnS_2 amount in the composites. The improvement of electrochemical properties of the composites compared with pure SnS_2 was attributed to the synergetic effects between graphene sheets and SnS_2.

Acknowledgments This work was supported by China Postdoctoral Science Foundation (no. 20100471296), Postdoctoral Foundation of Jiangsu Province (no. 1001003C), and National Nature Science Foundation of China (nos. 60928009, 61076017, and 60990314).

References

1. Kim HS, Chung YH, Kang SH, Sung YE (2009) Electrochim Acta 54:3606–3610
2. Zai JT, Wang KX, Su YZ, Qian XF, Chen JS (2011) J Power Sources 196:3650–3654
3. Patra CR, Odani A, Pol VG, Aurbach D, Gedanken A (2007) J Solid State Electrochem 11:186–194
4. Wang ZY, Chen G, Xia DG (2008) J Power Sources 184:432–436
5. Novoselov KS, Geim AK, Morozov SV, Jiang D, Zhang Y, Dubonos SV, Grigorieva IV, Firsov AA (2004) Science 306:666–669
6. Novoselov KS, Geim AK, Morozov SV, Jiang D, Katsnelson MI, Grigorieva IV, Dubonos SV, Firsov AA (2005) Nature 438:197–200
7. Yao J, Shen XP, Wang B, Liu HK, Wang GX (2009) Electrochem Commun 11:1849–1852
8. Wang XY, Zhou XF, Yao K, Zhang JG, Liu ZP (2011) Carbon 49:133–139
9. Wang GX, Wang B, Wang XL, Park J, Dou SX, Ahn H, Kim K (2009) J Mater Chem 19:8378–8384
10. Qiu DF, Xu ZJ, Zheng MB, Zhao B, Pan LJ, Pu L, Shi Y (2011) Graphene anchored with mesoporous NiO nanoplates as anode material for lithium-ion batteries. J Solid State Electrochem. doi:10.1007/s10008-011-1466-9
11. Du QL, Zheng MB, Zhang LF, Wang YW, Chen JH, Xue LP, Dai WJ, Ji GB, Cao JM (2010) Electrochim Acta 55:3897–3903
12. Hummers WS, Offeman RE (1958) J Am Chem Soc 80:1339–1339
13. Wu ZS, Ren WC, Wen L, Gao LB, Zhao JP, Chen ZP, Zhou GM, Li F, Cheng HM (2010) ACS Nano 4:3187–3194
14. Momma T, Shiraishi N, Yoshizawa A, Osaka T, Gedanken A, Zhu JJ, Sominski L (2001) J Power Sources 97–98:198–200
15. Kim TJ, Kim C, Son D, Choi M, Park B (2007) J Power Sources 167:529–535